

# Vorticity Dynamics in Isobarically Closed Porous Channels Part I: Standard Perturbations

J. Majdalani\*

Marquette University, Milwaukee, Wisconsin 53233

When acoustic pressure oscillations are induced in a porous channel of the closed–open type, the linearized Navier–Stokes equations can be solved analytically to obtain an accurate description of the temporal flowfield corresponding to laminar conditions. The channel considered here has a rectangular cross section, has two equally permeable walls, and is open at the downstream end. The current methodology parallels the closed–closed boundary analysis carried out previously for a channel with both ends closed. Limiting our scope to laminar conditions, we apply standard perturbation tools to present a closed-form solution that becomes asymptotically exact for large kinetic Reynolds numbers. Verifications are materialized by way of numerical simulations and quantification of the maximum absolute error entailed in the final formulations. Note that the error is found to exhibit a clear asymptotic behavior. Furthermore, the analytical formulation reveals vortical structures and explains the direct influence of acoustic pressure oscillations on the rotational waves generated in the closed–open configuration. Finally, the explicit roles of variable injection, viscosity, and oscillation frequency are explained.

## Nomenclature

$A$	=	dimensional oscillatory pressure amplitude
$a_s$	=	mean stagnation speed of sound, $\sqrt{(\gamma p_s/\rho_s)}$
$E_m$	=	maximum error in the asymptotic solution
$h$	=	channel half-height
$i$	=	root of complex numbers, $\sqrt{-1}$
$\mathbf{i}, \mathbf{j}, \mathbf{k}$	=	unit vectors in the Cartesian system
$K$	=	kinetic Reynolds number, $kh^2/\nu$
$k$	=	dimensional circular frequency, $(m - \frac{1}{2})\pi a_s/L$
$k_m$	=	wave number, $(m - \frac{1}{2})\pi h/L = kh/a_s$
$L$	=	internal chamber length
$l$	=	dimensionless chamber length, $L/h$
$M$	=	injection Mach number, $v_w/a_s$
$m$	=	pressure oscillation mode number
$p$	=	normalized pressure, $p^*/(\gamma p_s)$
$p_s$	=	mean chamber pressure, $\rho_s a_s^2/\gamma$
$p_1$	=	total unsteady pressure term, $p_1 = \hat{p} + \tilde{p}$
$Re$	=	crossflow Reynolds number, $v_w h/\nu = M Re$
$\overline{Re}$	=	acoustic Reynolds number, $a_s h/\nu$
$Sr$	=	Strouhal number, $kh/v_w = k_m/M$
$t$	=	dimensionless time, $t^* a_s/h$
$\mathbf{u}_0$	=	Taylor's profile normalized by $v_w$ , $(u_0, v_0)$
$\mathbf{u}_1$	=	total unsteady velocity term, $(\hat{\mathbf{u}} + \tilde{\mathbf{u}})$
$\hat{\mathbf{u}}, \tilde{\mathbf{u}}$	=	acoustic and vortical velocities, $\hat{\mathbf{u}}^*/a_s, \tilde{\mathbf{u}}^*/a_s$
$(u, v)$	=	axial and normal velocity components
$(u_0, v_0)$	=	$[(\pi/2)x \sin \theta, \cos \theta]$
$v_w$	=	normal injection speed at the wall
$x, y$	=	dimensionless axial and normal coordinates
$\gamma, \nu$	=	ratio of specific heats and viscosity
$\varepsilon$	=	reciprocal of the kinetic Reynolds number, $K^{-1}$
$\bar{\varepsilon}$	=	pressure wave amplitude, $A/(\gamma p_s)$
$\theta$	=	characteristic variable, $(\pi/2)y$
$\xi$	=	viscous parameter, $h\nu k^2 v_w^{-3}$
$\sigma$	=	reciprocal of the Strouhal number, $Sr^{-1}$
$\omega$	=	dimensionless vorticity, $\nabla \times \mathbf{u}$

## Subscripts

0, 1, ... = mean and temporal components

## Superscripts

Re, Im = real and imaginary parts, respectively  
\* = dimensional quantities

## Other symbols

- = variables in Euler's notation  
( ) = total quantities (mean and temporal)  
^ = acoustic terms  
~ = vortical terms

## I. Introduction

THE main focus of this work is to examine the time-dependent flowfield in a porous channel of the closed–open type. The goal is to develop analytical expressions for laminar flow variables that can help explain the acoustic character established in such a physical configuration. The presence of sidewall injection inside long and slender rectangular channels can lead to strong acoustic waves that are decreed by the system geometry. These waves can, in turn, interact with the channel's solid boundaries to generate time-dependent vorticity waves. The inevitable coupling between acoustic and vortical waves results in complex flow patterns that depend on the pressure oscillation mode shapes. The current analysis will attempt to characterize these flow patterns and unravel the main link between pressure oscillation mode shapes and vorticity production. In the process, the roles of variable injection, oscillation frequency, and viscosity will be indicated. Closed-form expressions for the velocity and vorticity fields will be formulized and verified numerically.

The work's technical merit lies in reproducing the analytical equations that help predict the unsteady flow motion inside porous channels that exhibit a closed–open configuration. The theoretical development to be pursued can be useful in increasing our understanding of unsteady flows entrained inside enclosures with transpiring walls. Applications include, but are not limited to, propulsion, surface ablation, filtration, and gas diffusion processes.

In propulsion related applications, numerous models have been developed over the years to simulate the internal flowfield inside solid rocket motors. The reader is referred to, for instance, Refs. 1 and 2 and the references therein. Some of these models have

Received 15 May 1999; presented as Paper 99-2503 at the AIAA/ASME/SAE/ASEE 35th Joint Propulsion Conference and Exhibit, Los Angeles, CA, 20–24 June 1999; revision received 18 January 2000; accepted for publication 20 January 2000. Copyright © 2000 by J. Majdalani. Published by the American Institute of Aeronautics and Astronautics, Inc., with permission.

\* Assistant Professor, Department of Mechanical and Industrial Engineering, Member AIAA.

attempted to simulate the ejection of gaseous substances from a propellant's burning surface by analyzing the expulsion of inert gases from transpiring surfaces. The advantages of such cold-flow models are twofold: 1) On the theoretical level, they allow for significant simplifications in the governing equations. 2) On the experimental level, they allow for prolonged data acquisition and reduce the hazards of experimentation associated with reactive substances.

In relation to the closed-open configuration, and in the spirit of modeling the oscillatory flowfield in rectangular channels with porous walls, recent experiments were conducted by Ma et al.,<sup>3,4</sup> Barron et al.,<sup>5</sup> Avalon et al.,<sup>6</sup> and Casalis et al.<sup>7</sup> Both Ma et al.<sup>3,4</sup> and Barron et al.<sup>5</sup> used sublimating carbon dioxide to simulate the ejected gases from rectangular slabs of dry ice. They also borrowed the concept of producing an oscillatory flow from Richardson and Tyler,<sup>8</sup> who used electric motors to control the motion of a piston reciprocating at the end of a crank. The main disparity between the Ma et al.<sup>3,4</sup> apparatus and that of Barron et al.<sup>5</sup> is that the latter used a Scotch-yoke to drive the piston, a condition that resulted in purer sinusoidal piston displacements.

More recently, Avalon et al.<sup>6</sup> and Casalis et al.<sup>7</sup> produced self-induced harmonic oscillations in their Veine d'Etude de la Couche Limite Acoustique facility. Theirs comprised a long channel with two counterfacing permeable and impermeable walls. Despite the meticulous effort of injecting air as uniformly as possible through the plane porous sections of their apparatus, small unavoidable fluctuations in the injectant rate led decidedly to the onset of a strong acoustic environment. In the aforementioned experiments, the placement of a choked orifice or nozzle at the downstream end determined whether the oscillation mode character was of the closed-closed or closed-open type. In the forthcoming analysis, we shall undertake the theoretical study of the laminar flow model stemming from pressure oscillations of the closed-open type.

The mathematical treatment unfolds in the following stages. Section II defines the geometry and mean flow stream function. It also provides the list of pertinent assumptions. The Navier-Stokes equations are subsequently linearized in Sec. III. The time-dependent field is decomposed in Sec. IV into acoustic and vortical components. Although the acoustic solution can be immediately characterized, the vortical solution requires a careful treatment and is deferred to Sec. V. Section V represents the essence of this paper, where a standard perturbation scheme will be applied to arrive at the desired solution. A companion paper will be devoted to two alternative techniques that apply to the momentum equation instead of the vorticity transport equation employed here. In Sec. VI, asymptotic results will be compared to numerical solutions of the linearized Navier-Stokes equations. In addition, the ensuing vortical structure will be closely examined. Last, the error associated with the asymptotic formulas will be quantified. For the reader's convenience, the procedure will be described with very few omissions despite its striking resemblance to Flandro's approach applied previously to the cylindrical tube.<sup>9</sup> The reason is that our current procedure contains subtle variations that lead to a cumulative error that differs from Flandro's.

## II. Defining the Basic Flow Model

### A. Porous Channel

We consider a long and slender rectangular channel of length  $L$  and width  $w$ . This channel is bounded by plane porous walls that are  $2h$  apart. Through these walls, a perfect gas is injected with constant uniform velocity  $v_w$ . Taking the height of the cross section to be smaller than the other two dimensions enables us to treat the problem as a case of two-dimensional flow. In fact, Terrill<sup>10</sup> (cf. pages 309 and 310) has shown that when the ratio of the width to the height of the channel is  $w/h \geq 4$ , one can justify ignoring the influence of passive side walls. For equal wall permeability, symmetry can be assumed about the meridian plane. As usual, symmetry reduces the solution domain by half. The preferred coordinate system is shown schematically in Fig. 1 with the origin at the porous wall. When spatial coordinates are normalized by  $h$ , the streamwise, transverse, and spanwise coordinates can be denoted by  $x$ ,  $y$ , and  $z$ . Disregarding the influence of rigid boundaries, we assume no variations in  $z$  and confine our solution to  $0 \leq x \leq l$  and  $0 \leq y \leq 1$ , where  $l = L/h$ .

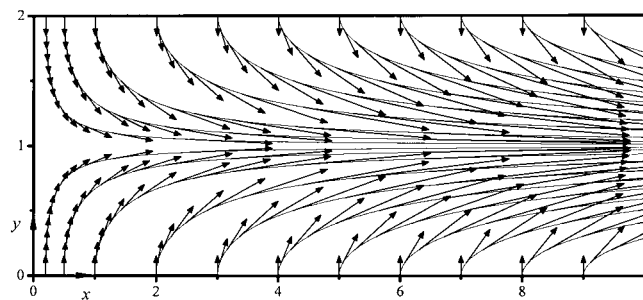


Fig. 1 System geometry showing select mean flow streamlines and velocity vector scales.

When the channel is closed at the fore end and open at the downstream end, small fluctuations in the injectant rate can give rise to acoustic pressure oscillations. These small pressure fluctuations can, in turn, couple with the mean flow and produce a time-dependent field that we wish to investigate. The streamlines shown in Fig. 1 correspond to typical flow patterns pertaining to the undisturbed state. The overlaying vector plot illustrates the spatial evolution of the mean velocity field.

### B. Limiting Conditions

For the mean flow, we consider a laminar, rotational, and incompressible regime where neither swirling nor mixing between incoming streams can take place. Additionally, a constant normal velocity is prescribed at the wall. For appreciable injection at the wall, we limit our scope to crossflow Reynolds numbers satisfying  $R = v_w h / \nu > 20$ , where  $\nu$  is the kinematic viscosity. The upper limit imposed on  $R$  is decreed by the need to maintain an injection Mach number  $M = v_w / a_s$  of order  $10^{-3}$ .

Regarding the acoustic pressure field, we constrain the oscillatory pressure amplitude  $A$  to remain small by comparison to the stagnation pressure  $p_s$  evaluated at  $x = 0$ . This enables us to construct another small parameter that scales with  $A/p_s$ . Finally, to break down the analysis into manageable pieces, we assume that the presence of isentropic oscillations does not affect the bulk fluid motion. Similar limiting conditions have been routinely used in the literature and may be traced back to Flandro's works.<sup>11,12</sup>

### C. Taylor's Flowfield

In the absence of small-amplitude disturbances, the steady Navier-Stokes equations can be solved exactly using a similarity transformation. As demonstrated by Berman,<sup>13</sup> when the steady stream function  $\Psi$  varies linearly, namely,

$$\Psi = -xF(y) \quad (1)$$

one can write  $(u_0, v_0) = (-xF', F)$ , where  $\mathbf{u}_0 = (u_0, v_0)$  is the mean velocity vector normalized by  $v_w$ . The separable component  $F$  must satisfy Berman's equation,  $F^{iv} + R(F'F'' - FF''') = 0$ , which depends on  $R$  and four boundary conditions:  $F'(0) = F(1) = F''(1) = 0$  and  $F(0) = 1$ . Although it may be possible to manage a time-dependent formulation for arbitrary  $F$ , we have decided to start by using a simple and practical solution corresponding to  $F = \cos[(\pi/2)y]$ . More sophisticated Berman functions can give rise to technical issues that tend to complicate and slightly obscure the forthcoming analysis. This solution, attributed to Taylor<sup>14</sup> or Yuan<sup>15</sup> has been thoroughly verified both numerically and experimentally to be a reasonable approximation for  $R > 20$ . In this range, Varapaev and Yagodkin<sup>16</sup> note minimal solution changes and almost no changes for  $R > 100$ . With this choice of  $F$ , the mean velocity and vorticity fields, namely,

$$\begin{aligned} \mathbf{u}_0 &= \{(\pi/2)x \sin[(\pi/2)y], \cos[(\pi/2)y]\} \\ \omega_0 &= -(\pi^2/4)x \cos[(\pi/2)y] \end{aligned} \quad (2)$$

satisfy all four boundary conditions. After normalizing the mean pressure by  $\gamma p_s$ , one integrates the momentum equation (given by

$$M^2 \mathbf{u}_0 \cdot \nabla \mathbf{u}_0 = -\nabla p_0 + \nabla^2 \mathbf{u}_0 / R \text{ to get}$$

$$p_0(x, y) = 1/\gamma - (M^2/2)((\pi^2/4)x^2\{1 + (\pi/2R) \sin[(\pi/2)y]\} + \cos^2[(\pi/2)y]) \quad (3)$$

Because the mean pressure depreciates in the streamwise direction, the channel length is limited to  $l < 100$ , for consistency in perturbation levels.

### III. Governing Equations

#### A. Normalized Navier-Stokes

Assuming constant kinematic viscosity and negligible bulk viscosity, the differential conservation of mass and momentum can be cast into the familiar nondimensional form

$$\frac{\partial \hat{p}}{\partial t} + \nabla \cdot (\hat{\rho} \hat{\mathbf{u}}) = 0 \quad (4)$$

$$\hat{\rho} \left[ \frac{\partial \hat{\mathbf{u}}}{\partial t} + (\hat{\mathbf{u}} \cdot \nabla) \hat{\mathbf{u}} \right] = -\nabla \hat{p} + \overline{Re}^{-1} \left[ \frac{4\nabla(\nabla \cdot \hat{\mathbf{u}})}{3} - \nabla \times (\nabla \times \hat{\mathbf{u}}) \right] \quad (5)$$

where the total instantaneous velocity  $\hat{\mathbf{u}}$  is normalized by the speed of sound  $a_s$  and the spatial coordinates by  $h$ , and where time is made dimensionless by reference to  $h/a_s$ , the average time it takes for a pressure disturbance to travel from the wall to the core. Using asterisks for dimensional variables, the instantaneous pressure and density can be referenced to stagnation conditions. Setting  $\hat{p} \equiv \hat{p}^*/(\gamma p_s)$  and  $\hat{\rho} \equiv \hat{\rho}^*/\rho_s$ , the acoustic Reynolds number  $\overline{Re}$  in Eq. (5) will be  $a_s h/\nu$ .

#### B. Perturbed Variables

When periodic oscillations are introduced at a radian frequency  $k$ , the instantaneous pressure can be written as a sum of its steady and acoustic components. Using subscripts for perturbation orders, the total pressure can be expanded into

$$\hat{p}^* = p_0^*(x^*, y^*) + p_1^*(x^*, y^*, t^*) = p_0^* + AP(x^*, y^*) \exp(-ikt^*) \quad (6)$$

where  $P$  is a spatial function of  $\mathcal{O}(1)$  that will be determined in Sec. IV.D. Normalizing and using  $p_0^* = p_s$ , one gets

$$\hat{p}(x, y, t) = 1/\gamma + \bar{\varepsilon} P(x, y) \exp(-ik_m t) + \mathcal{O}(M^2 x^2)$$

$$\cong 1/\gamma + \bar{\varepsilon} p_1(x, y, t) \quad (7)$$

where  $k_m = kh/a_s$  is the nondimensional frequency and  $\bar{\varepsilon} = A/(\gamma p_s)$  is the wave amplitude. Other fluctuating variables can be expanded in a similar fashion:

$$\hat{\rho}(x, y, t) = (\rho_s + \rho_1^*)/\rho_s = 1 + \bar{\varepsilon} \rho_1(x, y, t) \quad (8)$$

In much the same way, velocity lends itself to decomposition. Knowing the mean solution from Eqs. (2) and (3), we may follow Lighthill<sup>17</sup> by considering small velocity oscillations about the mean and write

$$\hat{\mathbf{u}}^*(x^*, y^*, t^*) = v_w \mathbf{u}_0(x^*, y^*) + \mathbf{u}_1^*(x^*, y^*, t^*) \quad (9)$$

Normalizing by  $a_s$  begets, for the velocity and vorticity companion,

$$\hat{\mathbf{u}}(x, y, t) = M \mathbf{u}_0(x, y) + \bar{\varepsilon} \mathbf{u}_1(x, y, t)$$

$$\hat{\omega}(x, y, t) = M \omega_0(x, y) + \bar{\varepsilon} \omega_1(x, y, t) \quad (10)$$

#### C. Total Field Decomposition

Inserting Eqs. (7–10) back into Eqs. (4) and (5) precipitates the zero-order expansion in the wave amplitude. Collecting terms of  $\mathcal{O}(\bar{\varepsilon})$ , the first-order linearized expansion of the fundamental equations is obtained:

$$\frac{\partial \rho_1}{\partial t} + \nabla \cdot \mathbf{u}_1 = -M \nabla \cdot (\rho_1 \mathbf{u}_0) \quad (11)$$

$$\frac{\partial \mathbf{u}_1}{\partial t} = -M [\nabla(\mathbf{u}_0 \cdot \mathbf{u}_1) - \mathbf{u}_1 \times (\nabla \times \mathbf{u}_0) - \mathbf{u}_0 \times (\nabla \times \mathbf{u}_1)]$$

$$- \nabla p_1 + \overline{Re}^{-1} \left[ \frac{4\nabla(\nabla \cdot \mathbf{u}_1)}{3} - \nabla \times (\nabla \times \mathbf{u}_1) \right] \quad (12)$$

This set incorporates the influence of bulk fluid motion on the time-dependent field. The same set was obtained previously, using a different notation, in the treatment of oscillatory flows in cylindrical tubes of the closed-closed type.<sup>1,12,18</sup>

### IV. Temporal Field Decomposition

#### A. Irrotational and Solenoidal Vectors

At this juncture, it is useful to decompose the time-dependent vector into an irrotational and a solenoidal component. As usual, using a circumflex to designate acoustic parts and a tilde for vortical parts, the time-dependent velocity component can be expressed as

$$\mathbf{u}_1 = \hat{\mathbf{u}} + \tilde{\mathbf{u}} \quad (13)$$

Similar decomposition has been successfully employed by Flandro.<sup>12</sup> Thus,

$$\omega_1 \equiv \nabla \times \mathbf{u}_1 = \tilde{\omega} \equiv \nabla \times \tilde{\mathbf{u}}, \quad p_1 = \hat{p}, \quad \rho_1 = \hat{\rho} \quad (14)$$

#### B. Linearized Navier-Stokes Equations

When Eqs. (13) and (14) are substituted back into Eqs. (11) and (12), two independent sets of formulas ensue. These are coupled through existing boundary conditions and are given by the following:

1) Acoustic set:

$$\frac{\partial \hat{p}}{\partial t} + \nabla \cdot \hat{\mathbf{u}} = -M \nabla \cdot (\hat{\rho} \mathbf{u}_0) \quad (15)$$

$$\frac{\partial \hat{\mathbf{u}}}{\partial t} = -\nabla \hat{p} + \frac{4\overline{Re}^{-1} \nabla(\nabla \cdot \hat{\mathbf{u}})}{3} - M [\nabla(\hat{\mathbf{u}} \cdot \mathbf{u}_0) - \hat{\mathbf{u}} \times (\nabla \times \mathbf{u}_0)] \quad (16)$$

2) Vortical set:

$$\nabla \cdot \tilde{\mathbf{u}} = 0 \quad (17)$$

$$\frac{\partial \tilde{\mathbf{u}}}{\partial t} = -\overline{Re}^{-1} \nabla \times (\nabla \times \tilde{\mathbf{u}}) - M [\nabla(\tilde{\mathbf{u}} \cdot \mathbf{u}_0) - \tilde{\mathbf{u}} \times (\nabla \times \mathbf{u}_0) - \mathbf{u}_0 \times (\nabla \times \tilde{\mathbf{u}})] \quad (18)$$

#### C. Boundary Conditions

In finding  $\mathbf{u}_1$ , both  $\hat{\mathbf{u}}$  and  $\tilde{\mathbf{u}}$  must be first determined and then superposed in a manner that correctly satisfies the auxiliary conditions. These comprise both the no-slip condition at the wall and symmetry about the core. No-slip requires that  $u_1(x, 0) = 0$ , or  $\hat{\mathbf{u}}(x, 0) + \tilde{\mathbf{u}}(x, 0) = 0$ . However, symmetry requires that  $\partial u_1(x, 1)/\partial y = 0$ .

#### D. Acoustic Solution

When  $\hat{p} = \hat{p}$  is utilized, standard manipulation of Eqs. (15) and (16) condenses the set into a single hyperbolic partial differential equation,

$$\frac{\partial^2 \hat{p}}{\partial t^2} - \nabla^2 \hat{p} = -\frac{4\overline{Re}^{-1} \nabla(\nabla \cdot \hat{\mathbf{u}})}{3} - M \left\{ \nabla \cdot \left( \mathbf{u}_0 \frac{\partial \hat{p}}{\partial t} \right) - \nabla^2(\hat{\mathbf{u}} \cdot \mathbf{u}_0) + \nabla \cdot [\hat{\mathbf{u}} \times (\nabla \times \mathbf{u}_0)] \right\} \quad (19)$$

At this juncture, a solution can be managed to  $\mathcal{O}(M)$  by applying separation of variables and the closed-open end conditions. Because

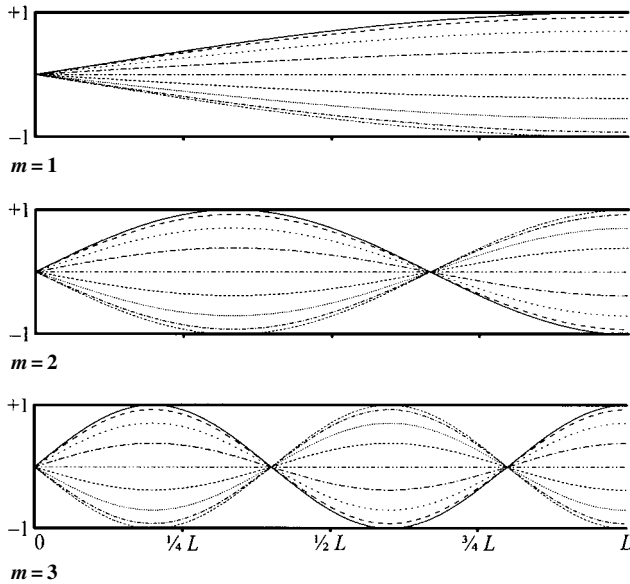


**Fig. 2** Acoustic velocity  $\hat{u}$  is profiled along the channel length at constant time intervals.

$l \gg 1$ , a solution to Eq. (19) can be retrieved from textbooks on wave propagation. Expressed in Euler's notation, the acoustic pressure is

$$\hat{p}(x, t) = \cos(k_m x) \exp(-ik_m t) + \mathcal{O}(M) \quad (20)$$

where the dimensionless wave number is given by  $k_m = kh/a_s = (m - \frac{1}{2})\pi/l$  where  $m = 1, 2, \dots, \infty$ . The corresponding frequency is  $f = (2m - 1)a_s/(4L)$ . The velocity companion can be integrated from Eq. (16) to render

$$\hat{u}(x, t) = i \sin(k_m x) \exp(-ik_m t) + \mathcal{O}(M) \quad (21)$$

Acoustic amplitudes stemming from Eq. (21) are shown in Fig. 2 for the first three oscillation mode shapes.

### E. Vortical Equations

Letting  $\bar{\mathbf{u}}(x, y) \equiv (\bar{u}, \bar{v})$ , and  $\bar{\boldsymbol{\omega}} \equiv \nabla \times \bar{\mathbf{u}} = \bar{\omega} \mathbf{k}$ , we use Euler's notation and write the vortical fluctuations as

$$\begin{aligned} \bar{\mathbf{u}}(x, y, t) &= \bar{\mathbf{u}}(x, y) \exp(-ik_m t) \\ \bar{\boldsymbol{\omega}}(x, y, t) &= \bar{\boldsymbol{\omega}}(x, y) \exp(-ik_m t) \end{aligned} \quad (22)$$

In lieu of Eqs. (17) and (18), we now have

$$\nabla \cdot \bar{\mathbf{u}} = 0 \quad (23)$$

$$i\bar{\mathbf{u}} = [\nabla(\bar{\mathbf{u}} \cdot \mathbf{u}_0) - \bar{\mathbf{u}} \times \boldsymbol{\omega}_0 - \mathbf{u}_0 \times \bar{\boldsymbol{\omega}}]/Sr + \nabla \times \bar{\boldsymbol{\omega}}/K \quad (24)$$

where

$$Sr = kh/v_w = (m - \frac{1}{2})(\pi h a_s / v_w L) \quad (25)$$

$$K = kh^2/v = (m - \frac{1}{2})(\pi h^2 a_s / v L) \quad (26)$$

The two emerging similarity parameters are the Strouhal number  $Sr$ , and the kinetic Reynolds number  $K$ . Practically, because the kinematic viscosity of most gases happens to be very small, the parametric variation in  $K$  reported by many researchers has fallen into the range  $10^4 < K < 10^8$ . Therefore, we define  $\varepsilon \equiv K^{-1}$  to be a primary perturbation parameter. For similar reasons, because unsteady flows are characterized by appreciable Strouhal numbers, we define  $\sigma = 1/Sr$ . Note that  $\varepsilon$  is always smaller than  $\sigma$  because the ratio  $\sigma/\varepsilon = v_w h/v$  is the crossflow Reynolds number  $R$ , which is large irrespective of frequency.

Subject to confirmation at the conclusion of the forthcoming analysis, we now make the conditional stipulation that  $\bar{v}/\bar{u} = \mathcal{O}(M)$ .

Being a smaller quantity,  $\bar{v}$  can be omitted at the first perturbation level with no effect on the solution desired at  $\mathcal{O}(M)$ . Therefore, Eq. (24) collapses at  $\mathcal{O}(M)$  into

$$i\bar{\mathbf{u}} = \sigma \left[ \frac{\partial}{\partial x} (\bar{\mathbf{u}} u_0) + v_0 \frac{\partial \bar{\mathbf{u}}}{\partial y} \right] - \varepsilon \frac{\partial^2 \bar{\mathbf{u}}}{\partial y^2}$$

or

$$i\bar{\mathbf{u}} = \sigma \left[ \frac{\partial}{\partial x} (\bar{\mathbf{u}} u_0) - v_0 \bar{\boldsymbol{\omega}} \right] + \varepsilon \frac{\partial \bar{\boldsymbol{\omega}}}{\partial y} \quad (27)$$

## V. Time-Dependent Vortical Field

### A. Vorticity Transport Equation

At present, we shall employ the vorticity transport equation to start with. In the companion paper, the solution will be based on the momentum equation and a unique choice of scaling arguments. Taking now the curl of Eq. (24) and using Eq. (22), the vorticity transport equation emerges:

$$i\bar{\boldsymbol{\omega}} = -\sigma \nabla \times (\bar{\mathbf{u}} \times \boldsymbol{\omega}_0 + \mathbf{u}_0 \times \bar{\boldsymbol{\omega}}) - \varepsilon \nabla^2 \bar{\boldsymbol{\omega}} + \mathcal{O}(M) \quad (28)$$

This can be rearranged in a scalar form that places leading-order terms on the left-hand side:

$$\frac{\partial \bar{\omega}}{\partial y} - \frac{i\bar{\omega}}{\sigma v_0} + \frac{u_0}{v_0} \frac{\partial \bar{\omega}}{\partial x} = -\frac{\bar{u}}{v_0} \frac{\partial \omega_0}{\partial x} + \frac{\varepsilon}{\sigma v_0} \left( \frac{\partial^2 \bar{\omega}}{\partial x^2} + \frac{\partial^2 \bar{\omega}}{\partial y^2} \right) \quad (29)$$

The right-hand side quantities representing the steady vorticity gradient and the viscous diffusion of time-dependent vorticity can be ignored at the first perturbation level. Physically, these terms symbolize viscous dissipation and axial convection of mean flow vorticity by virtue of the time-dependent vortical action. The latter is insignificant because of our original stipulation restricting unsteady flow effects on mean flow parameters to remain marginal. The third term on the left-hand side is retained, despite its misleading appearance of  $\mathcal{O}(M)$ , because it represents the downstream convection of vorticity. This phenomenon is vital to preserve the problem's physicality by providing an outlet to incoming vorticity. The base solution can now be achieved by expanding  $\bar{\omega}$  in powers of  $M$ , namely,  $\bar{\omega} = \omega_0 + M\omega_1 + \mathcal{O}(M^2)$ . Following substitution into Eq. (29), the leading-order term can be retrieved, by separation of variables, from

$$\frac{\partial \omega_0}{\partial y} - \frac{i\omega_0}{\sigma v_0} + \frac{u_0}{v_0} \frac{\partial \omega_0}{\partial x} = 0 \quad (30)$$

This, of course, must be contingent on satisfaction of both the no-slip condition at the wall and the no-flow restriction at the head end. Letting  $\omega_0 = X(x)Y(y)$ , Eq. (30) becomes

$$\frac{x}{X} \frac{dX}{dx} = -\frac{2}{\pi} \cot\left(\frac{\pi}{2}y\right) \frac{1}{Y} \frac{dY}{dy} + \frac{2i}{\pi\sigma} \csc\left(\frac{\pi}{2}y\right) = \lambda_n, \lambda_n > 0 \quad (31)$$

When we integrate and linearly sum over all possible solutions, the result is

$$\omega_0 = \sum_{\lambda_n} c_n \left[ x \cos\left(\frac{\pi}{2}y\right) \right]^{\lambda_n} \exp\left\{ \frac{2i}{\pi\sigma} \ell_n \tan\left[\frac{\pi}{4}(1+y)\right] \right\} \quad (32)$$

where  $\omega_0$  contains a denumerable set of arbitrary constants  $c_n$  associated with each  $\lambda_n$ . These must be specified in a manner to satisfy the no-slip condition at the wall, written for vorticity. The latter requires a delicate treatment and is covered next.

### B. Vorticity Boundary Condition

It is instructive to reduce Eq. (12), at  $\mathcal{O}(M)$ , into

$$\frac{\partial \mathbf{u}_1}{\partial t} = -M[\nabla(\mathbf{u}_1 \cdot \mathbf{u}_0) - \mathbf{u}_1 \times \boldsymbol{\omega}_0 - \mathbf{u}_0 \times \boldsymbol{\omega}_1] - \nabla p_1 - \overline{Re}^{-1} \nabla \times \boldsymbol{\omega}_1 \quad (33)$$

whose projection along  $x$  reads

$$\frac{\partial u_1}{\partial t} = -M \left[ \frac{\partial}{\partial x} (u_0 u_1 + v_0 v_1) - v_1 \omega_0 - v_0 \omega_1 \right] - \frac{\partial p_1}{\partial x} - \frac{1}{Re} \frac{\partial \omega_1}{\partial y} \quad (34)$$

Recalling that  $\omega_1 = \tilde{\omega}$ ,  $v_1 = \tilde{v}$ ,  $p_1 = \hat{p}$ , and that  $u_1(x, 0, t)$  must vanish to prevent slippage, Eq. (34) collapses, at the wall, into

$$0 = -M \left[ \frac{\partial}{\partial x} (\tilde{v} v_0) - \tilde{v} \omega_0 - v_0 \tilde{\omega} \right] - \frac{\partial \hat{p}}{\partial x} - \frac{1}{Re} \frac{\partial \tilde{\omega}}{\partial y} \quad (35)$$

Rearranging, and using  $\hat{p} = \cos(k_m x) \exp(-ik_m t)$ , the no-slip condition translates into

$$\tilde{\omega} = -Sr \sin(K_m x) \exp(-ik_m t) + \frac{Sr}{K} \frac{\partial \tilde{\omega}}{\partial y} + \mathcal{O}(M) \quad (36)$$

which can be recast into

$$\tilde{\omega}(x, 0) = -Sr \sin(K_m x) + \frac{Sr}{K} \frac{\partial \tilde{\omega}}{\partial y} + \mathcal{O}(M) \quad (37)$$

Equation (37) indicates that vorticity is most intense at wall locations given by  $x/l = (2n - 1)/(2m - 1)$ , where  $n \leq m$  represents the positive integral number of acoustic velocity maxima (shown in Fig. 2) for a given oscillation mode  $m$ . At these nodes,  $\hat{u}$  has maximum amplitude.

### C. Inviscid Vorticity

Equation (37) can now be used in conjunction with Eq. (32) to specify the separation eigenvalues:

$$\varpi_0(x, 0) = -Sr \sin(k_m x) \equiv -Sr \sum_{n=0}^{\infty} \frac{(-1)^n (k_m x)^{2n+1}}{(2n+1)!} \quad (38)$$

$$\lambda_n = 2n + 1, \quad c_n = -\frac{Sr (-1)^n (k_m)^{2n+1}}{(2n+1)!} \quad (39)$$

whence

$$\varpi_0(x, y) = Sr \left\{ \sum_{n=0}^{\infty} \frac{(-1)^n}{(2n+1)!} \left[ -k_m x \cos\left(\frac{\pi}{2} y\right) \right]^{2n+1} \right\} \\ \times \exp \left\{ \frac{2}{\pi} i Sr \ell_n \tan \left[ \frac{\pi}{4} (1+y) \right] \right\} \quad (40)$$

Recalling Taylor's mean flow stream function from Sec. II.C, we recognize that the infinite series between braces is a sine function of  $\Psi$ . At the outset, we let  $Z(x, y) \equiv k_m \Psi(x, y)$ , and simplify Eq. (40) into

$$\varpi_0(x, y) = Sr \sin(Z) \exp(-i\Phi_0) \quad (41)$$

where the temporal phase lead of the vortical wave is found to depend on

$$\Phi_0(y) = -(2/\pi) Sr \ell_n \tan[(\pi/4)(1+y)] \quad (42)$$

### D. Ideal Stream Function

We now resort to the time-dependent stream function  $\bar{s} = \psi \mathbf{k}$ , where  $\bar{\mathbf{u}} \equiv \nabla \times \bar{s}$ , to replace the velocity components via  $\bar{u} = \partial \psi / \partial y$  and  $\bar{v} = -\partial \psi / \partial x$ . Starting with the vorticity equation,

$$\bar{\omega} = \frac{\partial \bar{v}}{\partial x} - \frac{\partial \bar{u}}{\partial y} = -\frac{\partial^2 \psi}{\partial x^2} - \frac{\partial^2 \psi}{\partial y^2} \quad (43)$$

we then proceed heuristically by posing that  $\psi$  must possess the same axial dependence as  $\tilde{\omega}$ . Because we shall be using successive approximations, we set  $\psi_0 = \psi_c \varpi_0$  and substitute into Eq. (43).

Balancing leading-order terms implies that  $\psi_c = \sigma^2 \cos^2[(\pi/2)y]$  or

$$\psi_0 = \sigma \cos^2[(\pi/2)y] \sin\{-k_m x \cos[(\pi/2)y]\} \exp(-i\Phi_0) \quad (44)$$

Having determined the inviscid flow stream function, it follows that the companion velocity is

$$\bar{\mathbf{u}} = \{i \cos[(\pi/2)y] \sin(Z) \mathbf{i} + M \cos^3[(\pi/2)y] \cos(Z) \mathbf{j}\} \exp(-i\Phi_0) \quad (45)$$

### E. Viscous Multipliers

Subject to verification at the conclusion of this section, we state without proof that both  $\bar{\mathbf{u}}$  and  $\tilde{\omega}$  must possess the same axial dependence as their inviscid counterparts. This statement is materialized by setting

$$\bar{u}(x, y) = u_c(y) \sin(Z) \exp(-i\Phi_0)$$

$$\tilde{\omega}(x, y) = \varpi_c(y) \sin(Z) \exp(-i\Phi_0) \quad (46)$$

where viscous correction multipliers  $u_c$  and  $\varpi_c$  must be evaluated. After substitution into the full vorticity transport equation, given by Eq. (29), several terms cancel out except for lower-order terms and terms of  $\mathcal{O}(Sr^2)$ . Balancing leading-order terms demands that

$$\frac{d\varpi_c}{dy} + \xi \sec^3\left(\frac{\pi}{2}y\right) \varpi_c - \frac{\pi^2}{4} u_c = 0 \quad (47)$$

where  $\xi = k_m^2 / (M^3 Re)$  appears as a dynamic similarity parameter, chiefly in control of the viscous correction multiplier. In seeking a relationship between  $u_c$  and  $\varpi_c$ , we resort to Eq. (27) and find

$$u_c = \{i\sigma \cos[(\pi/2)y] + \xi \sigma^2 \sec[(\pi/2)y]\} \varpi_c \quad (48)$$

Inserting this formula into Eq. (47) leads to an ordinary differential equation in  $\varpi_c$ :

$$\frac{d\varpi_c}{dy} + \left[ \xi \sec^3\left(\frac{\pi}{2}y\right) - i\sigma \frac{\pi^2}{4} \cos\left(\frac{\pi}{2}y\right) \right] \varpi_c = 0 \quad (49)$$

which, after some algebra, gives

$$\varpi_c(y) = C \exp \zeta \quad (50)$$

where, by omitting the imaginary argument in  $\zeta$  of effective  $\mathcal{O}(\sigma^2)$ , we find

$$\zeta = -\xi \int_0^y v_0^{-3}(\tau) d\tau = -\xi \int_0^y F^{-3}(\tau) d\tau \\ = -\frac{1}{\pi} \xi \left[ \ell_n \tan \frac{\pi}{4} (1+y) + \sec\left(\frac{\pi}{2}y\right) \tan\left(\frac{\pi}{2}y\right) \right] \quad (51)$$

### F. Corrected Vorticity

The complex constant of integration  $C$  can be evaluated from the vorticity boundary condition at the wall as specified by Eq. (37). Updating  $\varpi_c$  gives, at  $\mathcal{O}(M, \sigma^2)$

$$C \{1 - \xi \sigma^2 [\zeta'(0) - i\Phi_0'(0)]\} \sin[Z(x, 0)] \exp[\zeta(0) - i\Phi_0(0)] \\ = -Sr \sin(k_m x) \quad (52)$$

where

$$\zeta'(0) = -\xi, \quad \Phi_0'(0) = -Sr, \quad \zeta(0) = \Phi_0(0) = 0 \quad (53)$$

Direct substitution gives  $C(1 - i\xi\sigma) = Sr + \mathcal{O}(\sigma^2)$ . Hence,

$$C^{\text{Re}} = \frac{Sr^3}{Sr^2 + \xi^2}, \quad C^{\text{Im}} = \frac{\xi Sr^2}{Sr^2 + \xi^2} \quad (54)$$

Backward substitution into Eqs. (50), (46), and (22) yields, at last,

$$\tilde{\omega}(x, y, t) = C \sin(Z) \exp(\zeta - i\Phi_0 - ik_m t) \quad (55)$$

### G. Axial Velocity with Viscous Corrections

In much the same way, the velocity corrective multiplier can be deduced from Eq. (48), namely,

$$u_c = \{i\sigma \cos[(\pi/2)y] + \xi\sigma^2 \sec[(\pi/2)y]\} C \exp \zeta \equiv iB \exp \zeta \quad (56)$$

where

$$B^{\text{Re}} = \sigma (C^{\text{Re}} v_0 + \xi \sigma C^{\text{Im}} / v_0), \quad B^{\text{Im}} = \sigma (C^{\text{Im}} v_0 - \xi \sigma C^{\text{Re}} / v_0) \quad (57)$$

so that  $\tilde{u}$  is soluble by backward substitution into Eqs. (46) and (22). At length, we find that

$$\tilde{u}(x, y, t) = iB \sin(Z) \exp(\zeta - i\Phi_0 - ik_m t) \quad (58)$$

### H. Transverse Velocity

In principle, the normal component  $\tilde{v}$  can be derived from continuity. In practice, this may prove difficult unless we proceed heuristically by first proposing an ansatz of the form

$$\tilde{v} = g(y) \cos\{-k_m x \cos[(\pi/2)y]\} \exp(\zeta - i\Phi_0 - ik_m t) \quad (59)$$

Later substitution into Eq. (17) furnishes  $g(y)$ . Setting  $\partial\tilde{v}/\partial y \equiv -\partial\tilde{u}/\partial x$ , we find, to leading order,  $g = MBv_0^2$ . Therefore,

$$\tilde{v}(x, y, t) = MBv_0^2 \cos(Z) \exp(\zeta - i\Phi_0 - ik_m t) \quad (60)$$

which lends support to the former stipulation contending that  $\tilde{v}/\tilde{u} = \mathcal{O}(M)$ .

### I. Final Time-Dependent Formulation

By the retracing of our steps, the meaningful components of time-dependent axial and normal velocity are recapitulated hereafter along with their vorticity companion:

$$u_1 = \sin(k_m x) \sin(k_m t) - (B^{\text{Re}} \sin \varphi - B^{\text{Im}} \cos \varphi) \times \exp \zeta \sin(k_m x \cos \theta) \quad (61)$$

$$v_1 = -Mv_0^2 (B^{\text{Re}} \cos \varphi + B^{\text{Im}} \sin \varphi) \exp \zeta \cos(k_m x \cos \theta) \quad (62)$$

$$\omega_1 = -(C^{\text{Re}} \cos \varphi + C^{\text{Im}} \sin \varphi) \exp \zeta \sin(k_m x \cos \theta) \quad (63)$$

where

$$\theta = (\pi/2)y, \quad \varphi = k_m t - (2/\pi)Sr \ell_n \tan(\pi/4 + \theta/2) \quad (64)$$

Because the acoustic motion is, in essence, driven by the oscillatory pressure field, the first term in Eq. (61) can be envisaged as the inviscid response to the fluctuating pressure, and the second term can be interpreted as the viscous and vortical response that disappears asymptotically with increasing distance from the wall.

## VI. Discussion

### A. Numerical Verification

To gain confidence in the asymptotic formulas based on Eq. (61), we rely on computer-generated numerics and numerics combined with physical arguments. To that end, we use a shooting method to handle the two-point boundary value problem posing itself via Eq. (27) and the two auxiliary conditions described in Sec. IV.C. Careful choices of initial guesses and direction of integration across the channel are often necessary to ensure convergence. Our preference is to estimate small nonzero values at the core and integrate backward using a seventh-order Runge-Kutta scheme until the no-slip condition at the wall is fulfilled. Uniform steps, albeit very minute ones, are found to be adequate for the most part. If the spatial grid is too coarse, then a numerical overflow occurs. Naturally, the numerical difficulty arises at large kinetic Reynolds numbers. This spurious numerical artifact, which can be prevented by grid

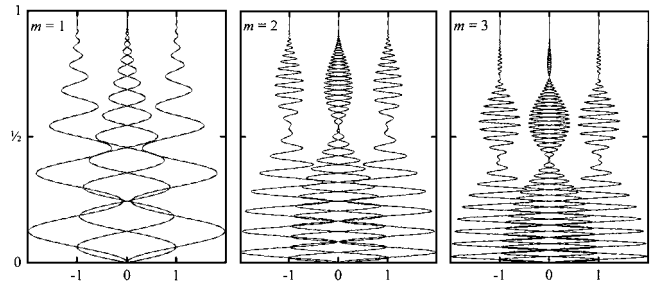


Fig. 3 Oscillatory axial velocity  $u_1$  vs  $y$  is shown at the downstream end ( $x=l$ ) for constant time intervals of  $\pi/2$ .

refinement, is ascribed to the increasing stiffness of the differential equation with  $K$ . Continual spatial grid refinement is, hence, necessary at successive increases in  $K$ . The number of grid points needed for convergence varied in our monitored routine from 10,000 to 20,000,000 points, but no effort was made to optimize the number by employing nonuniform meshes. If this were done, far fewer grid points would have been necessitated near the wall because the smaller steps are only required near the core to capture the exponentially depreciating vortical wavelength.

For typical values of the control parameters, the velocity's numerical solution is compared in Fig. 3 with its asymptotic counterpart evaluated from Eq. (61). For the first three oscillation modes, profiles are shown at four selected times of a complete cycle where  $Sr = 25(2m-1)$  and  $K = 10^6(2m-1)$ . In Fig. 3, asymptotics (full lines) and numerics (broken lines) are indistinguishable. For the fundamental mode,  $u_1$  starts at zero at the wall, in satisfaction of the velocity-adherence condition, then undergoes a velocity overshoot of twice the irrotational core amplitude. It then decays gradually to its inviscid form. This overshoot near the wall is a well-known feature of oscillatory flows that has been first reported by Richardson.<sup>19</sup> The observed doubling in amplitude takes place when vortical and acoustic waves happen to be in phase. This virtual 100% amplification is far more intense than the 13% overshoot described by Rott<sup>20</sup> (cf. page 402) and reported in laboratory experiments conducted, in the absence of wall injection, by Richardson<sup>19</sup> and Richardson and Tyler.<sup>8</sup>

For higher modes, similar damped waves are observed in the upstream portion delimited by the first internal velocity node. In the downstream portion, additional structures emerge. Specifically, a premature decay in the rotational wave is noted  $m-1$  times downstream of the  $m$ th velocity node. Such structures are depicted in Fig. 3 for  $m=2$  and 3 at the aft end. This axial station coincides with the location of the last pressure node where acoustic velocity amplitudes are largest. Beyond these premature rotational velocity nodes, the vortical field recuperates some strength before resuming its normal depreciation. To justify the presence of such intellectually challenging rotational nodes, a characterization of the time-dependent vortical structure is carried out. In the process, the influence of varying wall injection and viscosity is studied.

### B. Unsteady Vortical Structure

For  $m=1$ , Eq. (63) can be used to generate contour plots showing constant vorticity lines in percent of the maximum vorticity amplitude produced at the pressure nodes of the wall. When the frequency and kinematic viscosity are held constant, corresponding to a typical  $K = 10^6$  value, the Strouhal number can be modified by an order of magnitude by reducing the injectant rate. The corresponding vortical structures are shown in Fig. 4, for  $Sr = 10$  and 100. In particular, note in Fig. 4a the deeper vortical penetration with higher injection, and the downstream convection of vorticity, originating at the wall, that follows the mean flow streamlines. When injection is reduced in Fig. 4b, the irrotational region anchored at the core broadens out, resulting in a visible reduction in rotational depth.

When instead  $v_w$  and  $k$  are held constant, the effect of kinematic viscosity can be extrapolated in a similar fashion by varying  $K$ . We

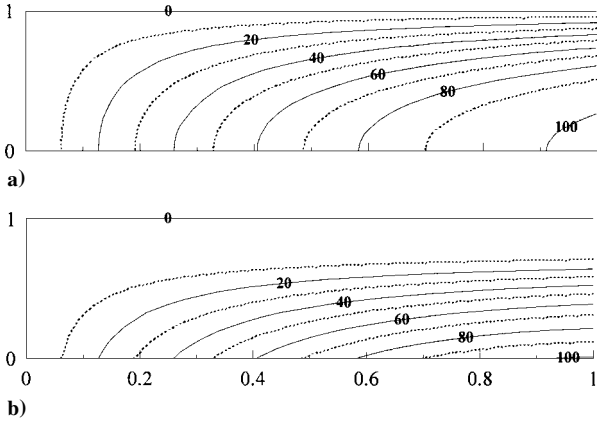


Fig. 4 Equispaced isovorticity lines shown in a)  $Sr=10$  and b)  $Sr=100$  where  $m=1$  and  $K=10^6$ .

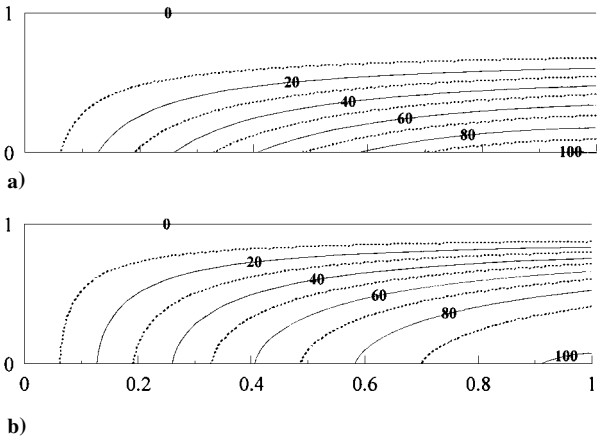


Fig. 5 Equispaced isovorticity lines shown in a)  $K=10^5$  and b)  $K=10^6$  where  $m=1$  and  $Sr=50$ .

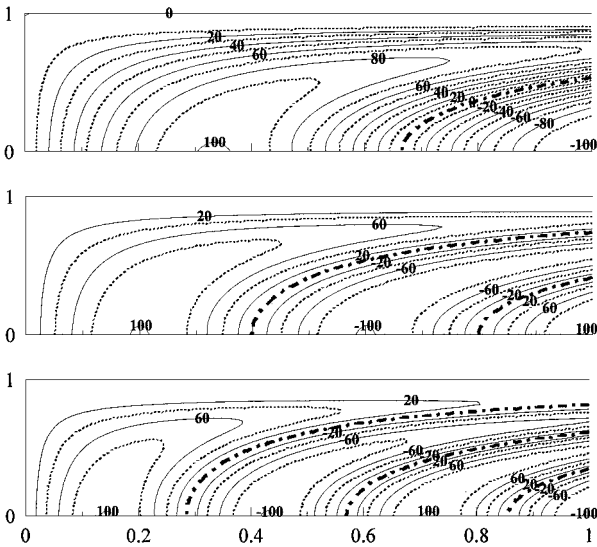


Fig. 6 Equispaced isovorticity lines shown for the first three harmonic modes when  $Sr=25(2m-1)$  and  $K=10^6(2m-1)$ .

find that, when viscosity is suppressed, as in Fig. 5, a wider and deeper spread of vorticity ensues. As such, one can envisage viscosity as an attenuation agent whose role is to resist the propagation of rotational waves. This is contrary to the role it plays in similar configurations with impermeable walls discussed, for example, in a survey by Rott<sup>20</sup> (cf. page 397).

As the oscillation mode evolves to  $m=2-4$ , isovorticity lines begin exhibiting interesting structures. These are shown in Fig. 6 for

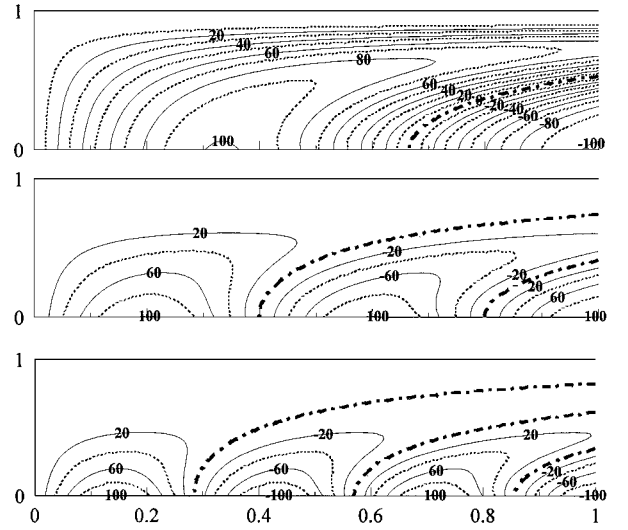


Fig. 7 Same as in Fig. 6 except that  $K=10^5(2m-1)$ ; this variation corresponds to an order of magnitude increase in kinematic viscosity.

typical values of the control parameters. In particular, these structures feature  $(m-1)$  lines of zero vorticity amplitude (chain curves), stemming from the acoustic pressure antinodes at the wall, for  $m > 1$ . These irrotational streaks partition the channel into  $m$  zones characterized by alternating directions of particle rotation. When crossing these delineation lines, vorticity changes sign and, therefore, direction. If we were to superimpose unsteady velocity profiles at discrete axial locations, we would find that the rotational nodes in  $u_1$  coincide precisely with the transverse location of the zero vorticity streaks. Apparently, as zero vorticity streaks drift downstream, they leave rotational nodes in the velocity fields that they intersect. Similar effects are noted in Fig. 7 when viscosity is increased. The result is a depreciation in both vortical wave propagation depth and amplitude at higher modes as well. Note, in particular, the broadening in the irrotational core by comparison to Fig. 6.

### C. Error Assessment

In arriving at the final asymptotic formulation set out in Eq. (61), a number of successive approximations were made that introduced uncertainty in the cumulative error entailed. Fortunately, the ultimate order verification of the error incurred in the derivation can be realized by applying a technique described by Bosley.<sup>21</sup> To that end, we define the maximum error  $E_m$  to be the maximum absolute difference between  $u_1$  given asymptotically and  $u_1^n$  computed numerically. Then for every  $m$ ,  $Sr$ , and  $\varepsilon$ , we can calculate, over a complete oscillation cycle,

$$E_m(m, Sr, \varepsilon) = \max_{\substack{0 \leq x \leq l \\ 0 \leq y \leq 1}} |u_1^n - u_1| \quad (65)$$

Suspecting that the error could be of  $\mathcal{O}(\varepsilon^\alpha)$ , we presuppose a functional variation of the form

$$E_m(m, Sr, \varepsilon) = \beta(m, Sr)\varepsilon^\alpha \quad (66)$$

and then determine the slope  $\alpha$  from the log-log plot of  $E_m$  vs  $\varepsilon$ . As in Fig. 8 for the first two acoustic oscillation modes, the slope of the maximum error approaches unity asymptotically. This result has been confirmed using the method of least squares in decreasing ranges of  $\varepsilon$ . The consistent asymptotic behavior is gratifying and, according to Bosley,<sup>21</sup> is indicative that our formulation is an honest and legitimate, uniformly valid expansion. This observation confirms that the error is of  $\mathcal{O}(\varepsilon)$ . We could not have done any better because  $\varepsilon = K^{-1}$  is the smallest naturally occurring perturbation parameter encountered heretofore. Because  $K^{-1} < Sr^{-1}$  at any oscillation frequency, the current procedure shows an improvement over its predecessor,<sup>9</sup> which exhibited an error of  $\mathcal{O}(Sr^{-1})$  (Refs. 22 and 23).

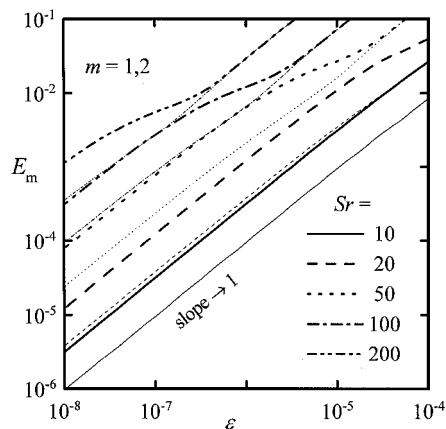


**Fig. 8** Asymptotic behavior of the maximum absolute error between numerical and asymptotic results for the first two acoustic oscillation modes; for each Strouhal number case, thicker curves correspond to  $m = 2$ .

## VII. Conclusions

This study focused on elucidating the nature of acoustico-vortical interactions in the porous channel with permeable walls. The scope was limited to laminar conditions to manage explicit formulations. To that end, issues regarding hydrodynamic stability and turbulence have been specifically excluded. The procedure was very similar to that used in analyzing the closed-closed channel configuration. Some of the main results included closed-form expressions for the time-dependent velocity and vorticity fields. These compared very favorably with numerical solutions to the linearized Navier-Stokes equations. Furthermore, they revealed the problem's similarity parameters and explained the relationship between acoustically excited oscillation modes and vortical production.

In the current paper, the solution was arrived at using successive approximations that applied to the vorticity transport equation. The numerical verification also relied on the linearized Navier-Stokes equations. In the forthcoming work, alternative analytical methods will be explored using WKB and multiple scale arguments. The formulations will be derived directly from the momentum equation and then compared to numerical simulations of the full, nonlinear, Navier-Stokes equations.

## References

- <sup>1</sup>Majdalani, J., and Van Moorhem, W. K., "Improved Time-Dependent Flowfield Solution for Solid Rocket Motors," *AIAA Journal*, Vol. 36, No. 2, 1998, pp. 241–248.
- <sup>2</sup>Majdalani, J., "Boundary-Layer Structure in Cylindrical Rocket Motors," *AIAA Journal*, Vol. 37, No. 4, 1999, pp. 505–508.
- <sup>3</sup>Ma, Y., Van Moorhem, W. K., and Shorthill, R. W., "Innovative Method of Investigating the Role of Turbulence in the Velocity Coupling Phenomenon,"

*Journal of Vibration and Acoustics*, Vol. 112, No. 4, 1990, pp. 550–555.

<sup>4</sup>Ma, Y., Van Moorhem, W. K., and Shorthill, R. W., "Experimental Investigation of Velocity Coupling in Combustion Instability," *Journal of Propulsion and Power*, Vol. 7, No. 5, 1991, pp. 692–699.

<sup>5</sup>Barron, J., Majdalani, J., and Van Moorhem, W. K., "A Novel Investigation of the Oscillatory Field over a Transpiring Surface," AIAA Paper 98-2694, June 1998.

<sup>6</sup>Avalon, G., Casalis, G., and Griffond, J., "Flow Instabilities and Acoustic Resonance of Channels with Wall Injection," AIAA Paper 98-3218, July 1998.

<sup>7</sup>Casalis, G., Avalon, G., and Pineau, J.-P., "Spatial Instability of Planar Channel Flow with Fluid Injection Through Porous Walls," *Physics of Fluids*, Vol. 10, No. 10, 1998, pp. 2558–2568.

<sup>8</sup>Richardson, E. G., and Tyler, E., "The Transverse Velocity Gradient Near the Mouths of Pipes in which an Alternating or Continuous Flow of Air is Established," *Proceedings of the Royal Society, London, Series A: Mathematical and Physical Sciences*, Vol. 42, No. 1, 1929, pp. 1–15.

<sup>9</sup>Flandro, G. A., "On Flow Turning," AIAA Paper 95-2530, July 1995.

<sup>10</sup>Terrill, R. M., "Laminar Flow in a Uniformly Porous Channel," *Aeronautical Quarterly*, Vol. 15, No. 3, 1964, pp. 299–310.

<sup>11</sup>Flandro, G. A., "Solid Propellant Acoustic Admittance Corrections," *Journal of Sound and Vibration*, Vol. 36, No. 3, 1974, pp. 297–312.

<sup>12</sup>Flandro, G. A., "Effects of Vorticity on Rocket Combustion Stability," *Journal of Propulsion and Power*, Vol. 11, No. 4, 1995, pp. 607–625.

<sup>13</sup>Berman, A. S., "Laminar Flow in Channels with Porous Walls," *Journal of Applied Physics*, Vol. 24, No. 9, 1953, pp. 1232–1235.

<sup>14</sup>Taylor, G. I., "Fluid Flow in Regions Bounded by Porous Surfaces," *Proceedings of the Royal Society, London, Series A: Mathematical and Physical Sciences*, Vol. 234, No. 1199, 1956, pp. 456–475.

<sup>15</sup>Yuan, S. W., "Further Investigation of Laminar Flow in Channels with Porous Walls," *Journal of Applied Physics*, Vol. 27, No. 3, 1956, pp. 267–269.

<sup>16</sup>Varapaev, V. N., and Yagodka, V. I., "Flow Stability in a Channel with Porous Walls," *Fluid Dynamics (Izvestiya Akademii Nauk SSSR, Mechanika Zhidkosti i Gaza)*, Vol. 4, No. 5, 1969, pp. 91–95.

<sup>17</sup>Lighthill, M. J., "The Response of Laminar Skin Friction and Heat Transfer to Fluctuations in the Stream Velocity," *Proceedings of the Royal Society, London, Series A: Mathematical and Physical Sciences*, Vol. 224, No. 1, 1954, pp. 1–23.

<sup>18</sup>Majdalani, J., and Van Moorhem, W. K., "A Multiple-Scales Solution to the Acoustic Boundary Layer in Solid Rocket Motors," *Journal of Propulsion and Power*, Vol. 13, No. 2, 1997, pp. 186–193.

<sup>19</sup>Richardson, E. G., "The Amplitude of Sound Waves in Resonators," *Proceedings of the Physical Society, London*, Vol. 40, No. 27, Section A, 1928, pp. 206–220.

<sup>20</sup>Rott, N., "Theory of Time-Dependent Laminar Flows," *High Speed Aerodynamics and Jet Propulsion—Theory of Laminar Flows*, edited by F. K. Moore, Vol. 4, Princeton Univ. Press, Princeton, NJ, 1964, pp. 395–438.

<sup>21</sup>Bosley, D. L., "A Technique for the Numerical Verification of Asymptotic Expansions," *SIAM Review*, Vol. 38, No. 1, 1996, pp. 128–135.

<sup>22</sup>Majdalani, J., Flandro, G. A., and Roh, T. S., "Implications of Unsteady Analytical Flowfields on Rocket Combustion Instability," AIAA Paper 98-3698, July 1998.

<sup>23</sup>Majdalani, J., Flandro, G. A., and Roh, T. S., "Convergence of Two Flowfield Models Predicting a Destabilizing Agent in Rocket Combustion," *Journal of Propulsion and Power*, Vol. 16, No. 3, 2000, pp. 492–497.